Enhanced voltage-controlled magnetic anisotropy via magnetoelasticity in FePt/MgO(001)

Qurat-ul-ain [1], D. Odkhuu,[2] S. H. Rhim,[1,*] and S. C. Hong [1,†]

[1]*Department of Physics and Energy Harvest-Storage Research Center, University of Ulsan, Ulsan 44610, Republic of Korea*
[2]*Department of Physics, Incheon National University, Incheon 22012, Republic of Korea*

The interplay between magnetoelectricity and magnetoelasticity (MEL) is studied in the context of voltage-controlled magnetic anisotropy (VCMA). Strain plays more than the role of changing lattice constants—that of the internal electric field in the heterostructure. As a prototype, FePt/MgO(001) is visited, where the behavior of two interfaces are drastically different: one exhibits switching, the other does not. Whether an external electric field (E_{ext}) is present or not, we found the VCMA coefficient larger than 1 pJ/(V m) as a consequence of the rearrangement of d orbitals with $m = \pm 1$ and ± 2 in response to an external electric field. In addition, magnetocrystalline anisotropy is analyzed with strain taken into account, where a nonlinear feature is presented, only accountable by invoking second-order MEL.

I. INTRODUCTION

The advent of spintronics has witnessed a realization of magnetic random access memory (MRAM), which compliments or replaces conventional memories. This progress has relied on giant magnetoresistance [1,2] and tunnel magnetoresistance [3,4]. Moreover, the advancement is further pushed forward with the incorporation of spin-transfer torque [5–7] and spin-orbit torque [8,9] for magnetization switching. In all cases, perpendicular magnetocrystalline anisotropy (PMA) is an essential ingredient to guarantee high bit density, lower switching current (I_{SW}), and thermal stability, $\Delta = KV/k_B T$, where K is anisotropy, k_B is the Boltzmann constant, and T is temperature. In spite of notable success in MRAM, high I_{SW} for switching and associated Joule heating are major obstacles to overcome.

Magnetoelectric random access memory has emerged as an alternative or compliment to MRAM, which utilizes voltage-controlled magnetic anisotropy (VCMA), where an external electric field (E_{ext}) manipulates switching from one magnetization state to the other. The efficiency of VCMA is characterized by a single parameter, the VCMA coefficient, $\beta = \Delta E_{MA}/\Delta E_{eff}$. The effective electric field, $E_{eff} = E_{ext}/\varepsilon_\perp$, where $\varepsilon_\perp$ is the out-of-plane component of the dielectric tensor of an insulator, and E_{MA} is the magnetocrystalline anisotropy (MA) energy. In the pursuit of VCMA, various heterostructures have been explored, where FePt/MgO is one choice. $L1_0$ FePt is ferromagnetic with a high Curie temperature of 750 K [10] and MgO has been widely used as substrate. In addition to E_{ext}, strain can be another driving force of VCMA, which influences β through $\varepsilon_\perp$ of the insulator *or* acts as an effective electric field at the ferromagnetic-insulator

interface even in the absence of E_{ext}. Hence, comparative studies of VCMA with and without strain would be intriguing.

In this paper, magnetoelectricity as well as magnetoelasticity (MEL) of FePt/MgO is investigated. The nonlinear MA as a function of strain (η) is explained by invoking second-order MEL contribution, which is usually ignored. The Fe interface shows spin reorientation for $4.5 < \eta < 7\%$ while, for the Pt case, MA is positive regardless of η. This difference stems from the competition between the positive effective anisotropy and negative first-order MEL. Later, extremely large β of FePt/MgO is presented as a result of an interplay between η and E_{ext}. More specifically, the rearrangement of d orbitals at the interface in response to E_{ext} is the key, whose details are analyzed with band- and atom-resolved decompositions of MA.

II. COMPUTATIONAL METHODS

First-principles calculations have been carried out using the Vienna ab initio Simulation Package [11] with projector augmented-wave basis [12]. Generalized gradient approximation is employed for the exchange-correlation potential [13]. Cutoff of 500 eV for plane wave expansion and a $12 \times 12 \times 1$ k mesh are used. Figure 1 shows the structure of bulk FePt and FePt/MgO film. Bulk FePt has $L1_0$ structure [Fig. 1(a)] while the film consists of five monolayers (MLs) of FePt on eight MLs of MgO(001) [Figs. 1(b) and 1(c)]. In film, two different interfaces are taken into account by placing (i) Fe atoms on top of O atoms [Fig. 1(b)] and (ii) Pt atoms on top of O atoms [Fig. 1(c)], which are referred to as Fe and Pt interfaces, respectively. The vacuum region of 12 Å is taken between adjacent cells. Both interfaces are systematically studied, where S, S-1, C, I, and I-1 refer to the surface, subsurface, center, interface, and subinterface layers, respectively. The optimized lattice constant of FePt and MgO are 3.864 and 4.212 Å, respectively, resulting in a large tensile strain (η) $\sim$8.2% on the FePt layer, assuming the

---

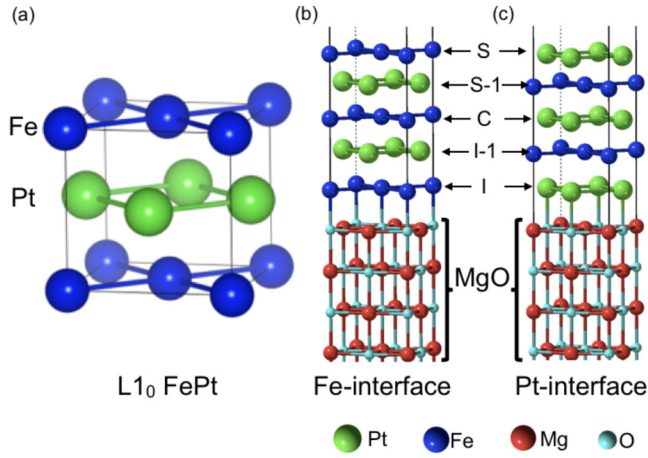*sonny@ulsan.ac.kr
†schong@ulsan.ac.kr

FIG. 1. (a) Bulk FePt $L1_0$ structure. 5 MLs of FePt on 8 MLs MgO (001) with (b) Fe and (c) Pt interfaces, respectively. Blue, green, cyan, and red spheres represent Fe, Pt, O, and Mg atoms, respectively. Surface, subsurface, center, interface, and subinterface layers are denoted by S, S-1, C, I, and I-1.

FIG. 2. E_{MA} as a function of η for (a) Fe and (b) Pt interfaces. Circles denote calculations and solid line represents fitting curve according to Eq. (2). Atomic layer decomposed E_{MA} for (c) Fe and (d) Pt interfaces, respectively. Blue, red, and black bars represent $\eta = 4, 6$ and 8%, respectively.

MgO substrate is unstrained. To study the strain-dependent MA of the system, η, defined as $(a - a_{FePt})/a_{FePt}$, is varied from 0% (unstrained FePt lattice constant) to 8% (nearly MgO lattice constant), where a_{FePt} is the equilibrium lattice constant of bulk FePt. Interlayer distances are relaxed for each strain with force criteria 1×10^{-3} eV/Å. MA energy (E_{MA}) is determined from the total energy difference between [100] and [001] directions, where spin-orbit coupling (SOC) is treated in a second-variational way [14]. Convergence of E_{MA} is checked with $30 \times 30 \times 1$ k mesh. The electric field along the surface normal is applied employing the dipole layer method [15]. In this paper, shape anisotropy is not included in magnetic anisotropy.

III. RESULTS AND DISCUSSION

When $\eta = 0\%$, $E_{MA} = 12.4$ and 21.5 erg/cm^2 for Fe and Pt interfaces, respectively, indicating perpendicular magnetization. Under tensile strain, both interfaces exhibit parabolic curves as shown in Fig. 2(a) and 2(b). However, one interface shows switching behavior but the other does not. For the Fe interface, $E_{MA} < 0$ for $4.5 < \eta < 7\%$, whereas for the Pt interface, E_{MA} decreases with strain. To check the validity of our calculations, E_{MA} of 5-ML and 9-ML FePt/MgO cases are compared for $\eta = 0\%$, where 5-ML turns out to be of appropriate thickness to reveal the interface, bulk-like, and surface effects. (See Fig. S1 in the Supplemental Material [16].)

The overall feature is expressed as

$$E_{MA} = E_{MA}^0 + b_1 t \sum_{k=1}^{3} \eta_k \alpha_k^2 + \frac{1}{2} B_1 t \sum_{k=1}^{3} \eta_k^2 \alpha_k^2, \quad (1)$$

where E_{MA}^0 is the zero-strain anisotropy energy per area; α_k and η_k ($k = 1, 2, 3$) are the direction cosines of magnetization and the strain tensor, respectively; t is the FM film thickness; b_1 and B_1 are the first- and second-order MEL coefficients, respectively [17,18].
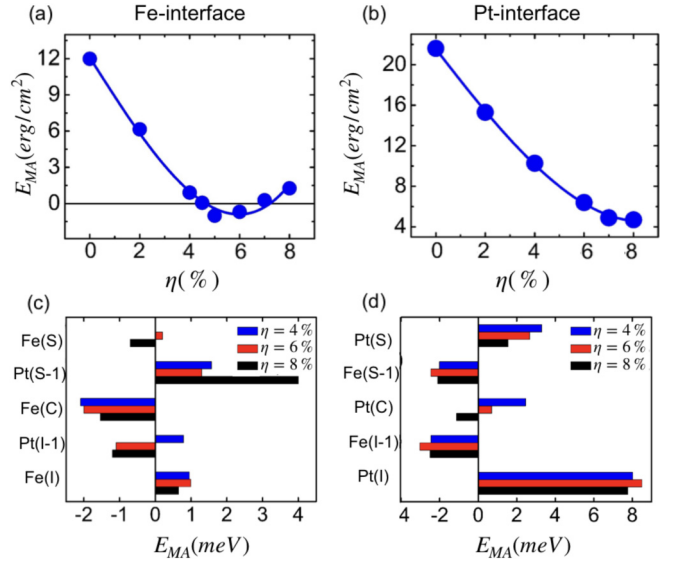
MEL energy is expanded up to second order of η, whose coefficient B_1 is usually small and ignored [19,20]. However, it is explicitly taken into account here, whose consequence is discussed later. The zero-strain anisotropy energy is approximated as $K_1 t (1 - \alpha_3^2)$ for uniaxial symmetry. It is decomposed into bulk and interface contributions, $K_1 = K_1^v + K_1^i/t \approx K_1^i/t$ for the thin film limit. In tetragonal structure, $\eta_1 = \eta_2 = \eta$ and the perpendicular strain η_3 is determined [21] from the magnetoelastic equation of state. Substituting the calculated strain value in Eq. (1) gives

$$E_{MA} = K_{eff} + (1 + \omega)b_1 t \eta + (1 - \omega)\frac{B_1}{2}t\eta^2, \quad (2)$$

where

$$K_{eff} = K_1^i + \omega \frac{b_1^2}{c_{11}}\left(1 + \frac{B_1}{2c_{11}}\right)t, \quad (3)$$

and

$$\omega = c_{11}^2/(c_{11} + B_1)^2, \quad (4)$$

where c_{11} is the elastic stiffness constant at constant magnetization. The derivation of Eq. (2) is also given in Supplemental Material [22].

Table I lists magnetoelastic and effective anisotropy coefficients, extracted by fitting *ab initio* results. The second-order

TABLE I. First-order (b_1) and second-order (B_1) bulk magnetoelastic coefficients in ($\times 10^8$ erg/cm^3) and effective anisotropy (K_{eff}) coefficient in (erg/cm^2) for Fe and Pt interfaces, respectively.

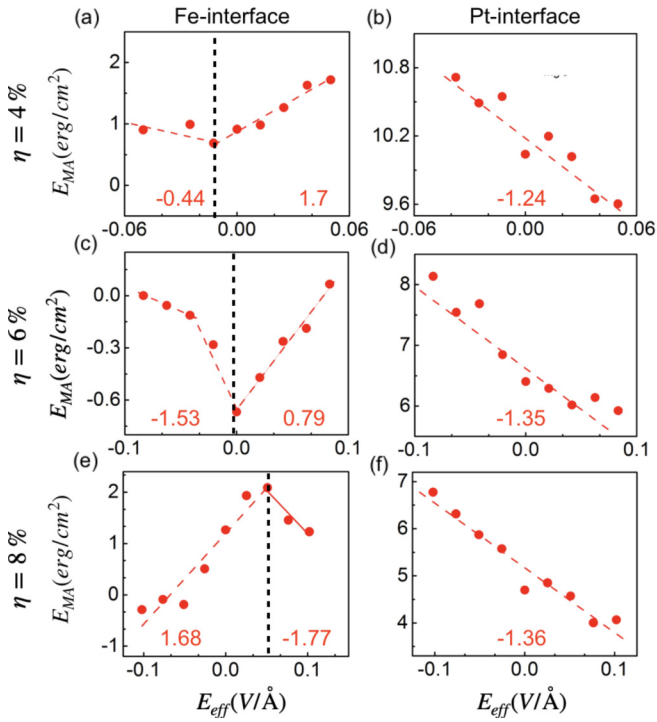| Interface	b_1	B_1	K_{eff}
Fe	−3.16	1.29	12.44
Pt	−2.43	0.79	21.57

FIG. 3. VCMA of FePt/MgO heterostructure at different strain values for Fe (left-panel) and Pt interfaces (right panel), respectively. Upper, middle, and lower rows represent strain (η) of 4, 6, and 8%, respectively. VCMA coefficient are denoted inside each plot.

FIG. 4. Orbital-resolved interfacial (a)–(c) Fe d bands for minority spin, (d)–(f) Pt d bands for majority spin along $\overline{X}$-$\overline{M}$-$\overline{\Gamma}$ at $\eta = 8\%$ under $E_{\text{eff}} = +76.5$ mV/Å, 0, -76.5 mV/Å. Blue, cyan, pink, and yellow for d_{xy}, $d_{x^2-y^2}$, d_{yz}, and d_{xz}. The d_{z^2} bands can contribute negatively to PMA and are not plotted here.

term, B_1, responsible for the nonlinearity is significantly large with 1.29 and 0.79 $\times 10^8$ erg/cm^3 for Fe and Pt interfaces, respectively. The difference in magnitudes of B_1 for both interfaces arises due to different local environments of two interfaces. Fe atoms experience larger MEL in the presence of a MgO substrate than the Pt interface. The differences of the two interfaces is further discussed now.

The calculated B_1 is of the opposite sign to that of b_1 for both interfaces. Further, it has been asserted that in the presence of strain, $b_1(\eta) = b_1 + B_1\eta$ [23,24]. In our study, the ratio $|B_1/b_1|$ is large for the Fe interface as compared to the Pt interface, leading to a change in sign of b_1 for large strain. For the Fe interface, a competition between K_{eff} and $b_1 t$ produces spin reorientation, for $4.5 < \eta < 7\%$. On the other hand, for the Pt interface, $K_{\text{eff}} > b_1 t$ results in PMA for η up to 8%.

Due to spin reorientation transition, we focus on $\eta = 4, 6,$ and 8%. Figures 2(c) and 2(d) provide atomic layer resolved E_{MA}. PMA mainly arises from Pt layers. Especially, the dominant PMA contribution comes from Pt(S-1) for the Fe interface and from Pt(I) for the Pt interface. Pt contribution to PMA is consistent with hard x-ray photoemission experiments [25]. On the contrary, Fe atoms mostly contribute to $E_{\text{MA}} < 0$, except Fe(I) and Fe(S) layers. Under strain, the overall behavior of E_{MA} remains the same for most of the atoms with changes in magnitude only. PMA from Fe(S), Pt(I-1), and Pt(C) at $\eta = 4\%$ becomes in plane as η approaches to 8%.

Now switching to VCMA, Fig. 3 shows change in MA as a function of E_{eff} for $\eta = 4, 6,$ and 8%. VCMA coefficient is defined as $\beta = \Delta E_{\text{MA}}/\Delta E_{\text{eff}}$ in the linear regime of E_{eff} as
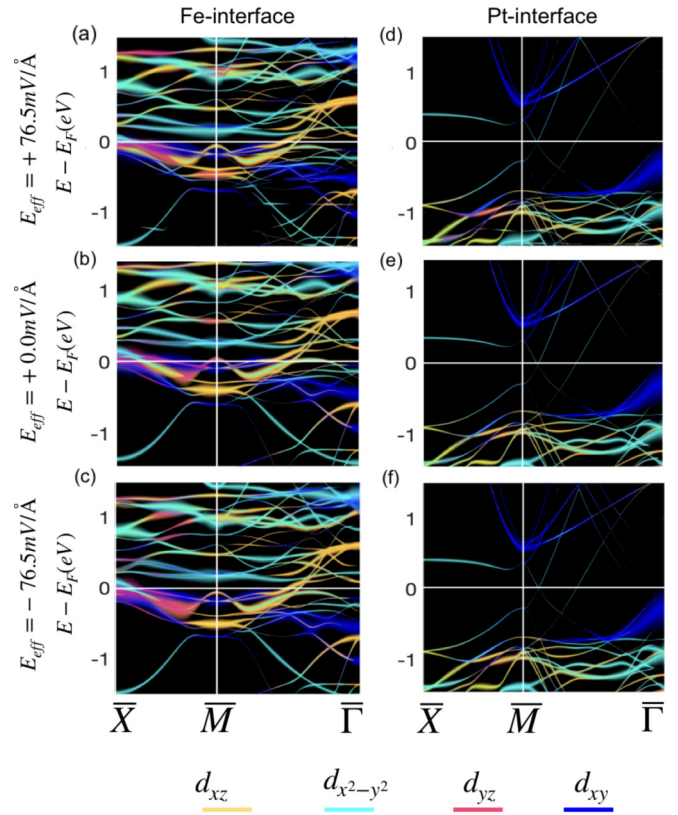
mentioned earlier. We choose $\epsilon_{\perp}/\epsilon_o = 20.0, 12.0, 9.8$ for MgO when $\eta = 4, 6,$ and 8%, respectively, taken from Ref. [26]. Large VCMA coefficients are found for both interfaces. For the Pt interface, $\beta = -1.24, -1.35,$ and -1.36 pJ/(V m) under $\eta = 4, 6,$ and 8%, respectively. On the other hand, the Fe interface exhibits qualitatively different VCMA with strain. The V-shape curve is apparent for $\eta = 4$ and 6% with $\beta = 1.70 \; (-0.44)$ and $0.79 \; (-1.53)$ pJ/(V m) when $E_{\text{eff}} > 0 \; (E_{\text{eff}} < 0)$, respectively. At $\eta = 8\%$, the VCMA curve changes shape with $\beta = -1.77 \; (1.68)$ pJ/(V m) under $E_{\text{eff}} > 0 \; (E_{\text{eff}} < 0)$.

To understand the underlying mechanism of strain-induced MA and VCMA, orbital-resolved bands at $\eta = 8\%$ are plotted in Fig. 4 along high-symmetry lines in two-dimensional Brillouin zone (BZ) under $E_{\text{eff}} = +76.5, 0,$ and -76.5 mV/Å. The $\eta = 8\%$ case is discussed in detail as it shows the largest VCMA coefficient. For Fe and Pt interfaces, only the minority spin channel of Fe d bands and majority spin channel of Pt d bands are presented, respectively, as other spin channels do not contribute significantly to PMA. The d_{z^2} orbitals for both interfaces can contribute negatively to PMA and are shown in the Supplemental Material [27]. Both spin channels for Fe and Pt d bands at $\eta = 8\%, 6\%,$ and 4% are also provided in Figs. S2 and S3 in the Supplemental Material, respectively.

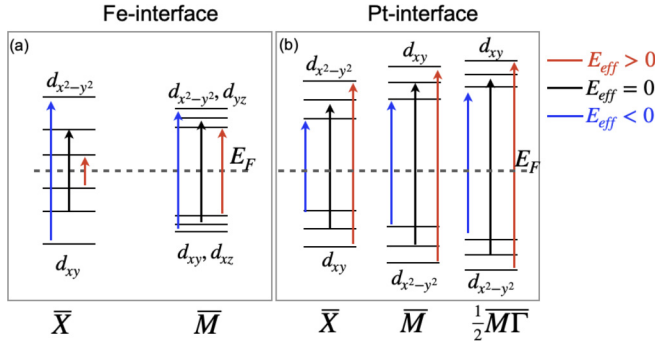In the framework of perturbation theory [28], positive (negative) E_{MA} comes from SOC between the unoccupied

FIG. 5. Schematic diagram of bands shift under E_{eff}. Here, the energy difference between occupied (e_o) and unoccupied (e_u) bands are used to calculate the strength of SOC (Δ); i.e., $\Delta^\alpha = \frac{1}{e_u - e_o}$, where $\alpha = +, 0, -$ represents $E_{\text{eff}} > 0$, $E_{\text{eff}} = 0$, and $E_{\text{eff}} < 0$, respectively. Vertical arrows indicate possible coupling responsible for PMA.

and occupied majority or minority spin states with the same (different) magnetic quantum number through $\ell_z(\ell_x)$. This approach has been widely applied in various systems [29–34].

First, we discuss without E_{ext}, namely, strain-induced MA. For the Fe interface, $E_{\text{MA}} > 0$ arises from $\langle d_{xy} \downarrow |\ell_z| d_{x^2-y^2} \downarrow \rangle$ and $\langle d_{xz} \downarrow |\ell_z| d_{yz} \downarrow \rangle$ along $\overline{XM}$ [Fig. 4(b)]. Similarly, for the Pt interface, $E_{\text{MA}} > 0$ mainly comes from $\langle d_{x^2-y^2} \uparrow |\ell_z| d_{xy} \uparrow \rangle$ along $\overline{M\Gamma}$ [Fig. 4(e)]. As tensile strain decreases, d bands experience overall downward shift for the Fe interface. However, for the Pt interface, d_{xy} and $d_{x^2-y^2}$ moves upward and downward, respectively, with decreasing strain, which is shown in Figs. S2 and S3 in the Supplemental Material [35]. Strain driven band rearrangement leads to substantial change in E_{MA} as $E_{\text{MA}} \propto \Delta = 1/(e_u - e_o)$, where e_u (e_o) denotes energies of unoccupied (occupied) bands. In particular, at $\eta = 6\%$ for the Fe interface, $E_{\text{MA}} < 0$ comes from $\langle d_{yz} \downarrow |\ell_x| d_{xy} \downarrow \rangle$ around $\frac{1}{2}\overline{XM}$. Also, at $\eta = 8\%$, $E_{\text{MA}} > 0$ is through $\langle d_{xy} \downarrow |\ell_z| d_{x^2-y^2} \downarrow \rangle$ around $\overline{X}$.

Moving to VCMA, band shifts at $\eta = 8\%$ under $E_{\text{eff}} = \pm 76.5$ mV/Å are shown in the top and bottom panels of Fig. 4. To understand in a simple picture, a schematic diagram is illustrated in Fig. 5. $\Delta^\alpha = 1/(e_u - e_o)$ ($\alpha = +, 0, -$) denotes the inverse of the energy difference between unoccu-

pied and occupied bands when $E_{\text{eff}} > 0$, $E_{\text{eff}} = 0$, and $E_{\text{eff}} < 0$, respectively.

Summing all SOC matrices, $\Delta^+ > \Delta^0 > \Delta^-$ justifies the shape of VCMA for the Fe interface. Under zero field, occupied d_{xy} (d_{xz}) bands couple with unoccupied $d_{x^2-y^2}$ (d_{yz}) bands at $\overline{X}$ and $\overline{M}$ points, giving $E_{\text{MA}} > 0$. Moreover, when $E_{\text{eff}} > 0$, d_{xy} and d_{xz} occupied bands along with $d_{x^2-y^2}$ and d_{yz} unoccupied bands move toward E_F at $\overline{X}$ and $\overline{M}$, providing large PMA while, when $E_{\text{eff}} < 0$, these bands moves away from E_F, as a result contributing small PMA. On the other hand, for the Pt interface, $\Delta^- > \Delta^0 > \Delta^+$ explains linear VCMA. When $E_{\text{eff}} < 0$, the unoccupied d_{xy} band and occupied $d_{x^2-y^2}$ band at $\overline{X}$ shift toward E_F with respect to zero field, resulting in enhanced PMA. However, when $E_{\text{eff}} > 0$, both these bands move away from E_F as compared to zero field, hence PMA is reduced.

IV. CONCLUSIONS

In summary, we investigated strain-dependent VCMA for both Fe and Pt interfaces of FePt/MgO(001) film using *ab initio* electronic-structure calculations. We predicted a huge VCMA coefficient ~ 1.77 pJ/(V m) due to the internal electric field as a result of strain. Moreover, MA as a function of strain is also discussed. The strain-dependent nonlinear MA is explained by invoking the second-order MEL term in MA energy. The Fe interface shows spin reorientation for $4.5 < \eta < 7\%$ as a consequence of the competition between the positive K_{eff} and negative $b_1 t$. MA turns out to be extremely sensitive to strain and interface. Our finding provides a direction for experiments to achieve enhanced VCMA coefficients along with large PMA for ultralow power nonvolatile memory devices.

[1] G. Binasch, P. Grünberg, F. Saurenbach, and W. Zinn, Phys. Rev. B **39**, 4828 (1989).

[2] M. N. Baibich, J. M. Broto, A. Fert, F. Nguyen Van Dau, F. Petroff, P. Etienne, G. Creuzet, A. Friederich, and J. Chazelas, Phys. Rev. Lett. **61**, 2472 (1988).

[3] M. Julliere, Phys. Lett. A **54**, 225 (1975).

[4] S. S. Parkin, C. Kaiser, A. Panchula, P. M. Rice, B. Hughes, M. Samant, and S.-H. Yang, Nat. Mater. **3**, 862 (2004).

[5] J. C. Slonczewski, J. Magn. Magn. Mater. **159**, L1 (1996).

[6] L. Berger, Phys. Rev. B **54**, 9353 (1996).

[7] M. Tsoi, A. Jansen, J. Bass, W.-C. Chiang, V. Tsoi, and P. Wyder, Nature **406**, 46 (2000).

[8] Y.-W. Oh, S.-h. C. Baek, Y. M. Kim, H. Y. Lee, K.-D. Lee, C.-G. Yang, E.-S. Park, K.-S. Lee, K.-W. Kim, G. Go *et al.*, Nat. Nanotechnol. **11**, 878 (2016).

[9] X. Qiu, P. Deorani, K. Narayanapillai, K.-S. Lee, K.-J. Lee, H.-W. Lee, and H. Yang, Sci. Rep. **4**, 4491 (2014).

[10] D. Xu, C.-J. Sun, J.-S. Chen, T.-J. Zhou, S. M. Heald, A. Bergman, B. Sanyal, and G. M. Chow, J. Appl. Phys. **116**, 143902 (2014).

[11] G. Kresse and J. Furthmüller, Phys. Rev. B **54**, 11169 (1996).

[12] P. E. Blöchl, Phys. Rev. B **50**, 17953 (1994).

[13] J. P. Perdew and Y. Wang, Phys. Rev. B **45**, 13244 (1992).

[14] D. Koelling and B. Harmon, J. Phys. C: Solid State Phys. **10**, 3107 (1977).

[15] J. Neugebauer and M. Scheffler, Phys. Rev. B **46**, 16067 (1992).

[16] See Supplemental Material at http://link.aps.org/supplemental/ 10.1103/PhysRevB.101.214436 for the layer-resolved E_{MA} of 5-ML and 9-ML FePt/MgO at zero strain to study the pure

thickness effect. One can see immediately that layer-resolved E_{MA} of both cases show similar trends. From this result, we can infer that our main conclusion does not change even if FePt film gets thicker.

[17] L. D. Landau and E. M. Lifshitz, *Electrodynamics of Continuous Media* (Pergamon, Oxford, 1984).

[18] D. Eastman, Phys. Rev. **148**, 530 (1966).

[19] A. B. Shick, D. L. Novikov, and A. J. Freeman, Phys. Rev. B **56**, R14259 (1997).

[20] V. Z. Paes and D. H. Mosca, J. Magn. Magn. Mater. **330**, 81 (2013).

[21] D. Sander, Rep. Prog. Phys. **62**, 809 (1999).

[22] See Supplemental Material at http://link.aps.org/supplemental/10.1103/PhysRevB.101.214436 for the derivation of magnetocrystalline anisotropy energy density in the presence of strain.

[23] M. Komelj and M. Fähnle, J. Magn. Magn. Mater. **222**, 245 (2000).

[24] Z. Tian, D. Sander, and J. Kirschner, Phys. Rev. B **79**, 024432 (2009).

[25] S. Ueda, M. Mizuguchi, Y. Miura, J. Kang, M. Shirai, and K. Takanashi, Appl. Phys. Lett. **109**, 042404 (2016).

[26] P. V. Ong, N. Kioussis, D. Odkhuu, P. Khalili Amiri, K. L. Wang, and G. P. Carman, Phys. Rev. B **92**, 020407(R) (2015).

[27] See Supplemental Material at http://link.aps.org/supplemental/10.1103/PhysRevB.101.214436 for the orbital-resolved band structure of d bands of Fe and Pt atoms including d_{z^2}, which is not shown in the main text. The d_{z^2} mainly couples with $d_{xz/yz}$ in the minority spin channel through l_x yielding in-plane MA around $\overline{M}$ for Fe and around $\overline{X}$ for Pt atom.

[28] D. S. Wang, R. Wu, and A. J. Freeman, Phys. Rev. B **47**, 14932 (1993).

[29] K. Nakamura, T. Akiyama, T. Ito, M. Weinert, and A. J. Freeman, Phys. Rev. B **81**, 220409(R) (2010).

[30] D. Odkhuu, W. S. Yun, S. H. Rhim, and S. C. Hong, Appl. Phys. Lett. **98**, 152502 (2011).

[31] D. Odkhuu, S. H. Rhim, N. Park, and S. C. Hong, Phys. Rev. B **88**, 184405 (2013).

[32] K. Hotta, K. Nakamura, T. Akiyama, T. Ito, T. Oguchi, and A. J. Freeman, Phys. Rev. Lett. **110**, 267206 (2013).

[33] D. Odkhuu, W. S. Yun, S. H. Rhim, and S. C. Hong, J. Magn. Magn. Mater. **414**, 126 (2016).

[34] Qurat-ul-ain, D. D. Cuong, D. Odkhuu, S. H. Rhim, and S. C. Hong, J. Magn. Magn. Mater. **467**, 69 (2018).

[35] See Supplemental Material at http://link.aps.org/supplemental/10.1103/PhysRevB.101.214436 for the majority and minority spin state of Fe and Pt d bands along high symmetry direction in 2D Brilliouin zone. A comparison of band shift under 8, 6, and 4% strain is provided.